

Stress-Induced Dinoflagellate Bioluminescence at the Single Cell Level

Mazyar Jalaal^{1,2}, Nico Schramma^{1,2}, Antoine Dode^{1,3}, H el ene de Maleprade¹,

Christophe Raufaste^{1,4}, Raymond E. Goldstein¹

¹*Department of Applied Mathematics and Theoretical Physics,*

University of Cambridge, Cambridge CB3 0WA, United Kingdom

²*Max-Planck Institute for Dynamics and Self-Organization, G ottingen, Germany*

³* cole Polytechnique, 91128 Palaiseau Cedex, France*

⁴*Universit e C te d'Azur, CNRS, Institut de Physique de Nice, CNRS, 06100 Nice, France*

(Dated: March 20, 2020)

One of the characteristic features of many marine dinoflagellates is their bioluminescence, which lights up nighttime breaking waves or seawater sliced by a ship's prow. While the internal biochemistry of light production by these microorganisms is well established, the manner by which fluid shear or mechanical forces trigger bioluminescence is still poorly understood. We report controlled measurements of the relation between mechanical stress and light production at the single-cell level, using high-speed imaging of micropipette-held cells of the marine dinoflagellate *Pyrocystis lunula* subjected to localized fluid flows or direct indentation. We find a viscoelastic response in which light intensity depends on both the amplitude and rate of deformation, consistent with the action of stretch-activated ion channels. A phenomenological model captures the experimental observations.

Bioluminescence, the emission of light by living organisms, has been a source of commentary since ancient times [1], from Aristotle and Pliny the Elder, to Shakespeare and Darwin [2], who, like countless mariners before him, observed of the sea, "... every part of the surface, which during the day is seen as foam, now glowed with a pale light. The vessel drove before her bows two billows of liquid phosphorus, and in her wake she was followed by a milky train. As far as the eye reached, the crest of every wave was bright,...". The glow Darwin observed arose most likely from bacteria or dinoflagellates, unicellular eukaryotes found worldwide in marine and freshwater environments.

Bioluminescence is found in a large range of organisms, from fish to jellyfish, worms, fungi, and fireflies. While discussion continues regarding the ecological significance of light production [3], the *internal* biochemical process that produces light is now well understood. In the particular case of dinoflagellates [4], changes in intracellular calcium levels produce an action potential, opening voltage-gated proton channels in the membranes of organelles called *scintillons*, lowering the pH within them [5] and causing oxidation of the protein *luciferin*, catalyzed by *luciferase*. Far less clear is the mechanism by which fluid motion triggers bioluminescence.

Early experiments on light emission utilizing unquantified fluid stirring or bubbling [6] were superseded over the past two decades by studies in the concentric cylinder geometry of Couette flow [7, 8] and macroscopic contracting flows [9, 10]. Subsequent experiments explored light production by cells carried by fluid flow against barriers in microfluidic chambers [11], or subjected to the localized forces of an atomic force microscope [12]. From these have come estimates of the stress needed to trigger light production. Indeed, dinoflagellates can serve as probes of shear in fluid flows [7, 9, 13–16]. At the molecular

level, biochemical interventions have suggested a role for stretch-activated ion channels [17] —known to feature prominently in touch sensation [18]—leading to the hypothesis that fluid motion stretches cellular membranes, forcing channels open and starting the biochemical cascade that produces light.

Here, as a first step toward an in-depth test of this mechanism, we study luminescence of single cells of the dinoflagellate *Pyrocystis lunula* (Fig. 1) induced by precise mechanical stimulation. The cellular response is found to be 'viscoelastic', in that it depends not only on the amplitude of cell wall deformation but also on its rate. A phenomenological model linking this behavior to light production provides a quantitative account of these observations.

P. lunula is an excellent organism for the study of bioluminescence because its large size ($\sim 40 \mu\text{m}$ in diameter and $\sim 130 \mu\text{m}$ in length), lack of motility as an adult, rigid external cell wall and negative buoyancy all facil-

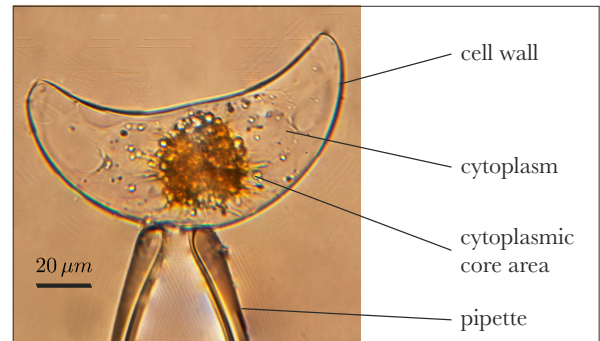


FIG. 1. The unicellular marine dinoflagellate *Pyrocystis lunula*, held on a glass micropipette. Chloroplasts (yellow/brown) are in the cytoplasmic core at night and the crescent-shaped cell wall encloses the cell.

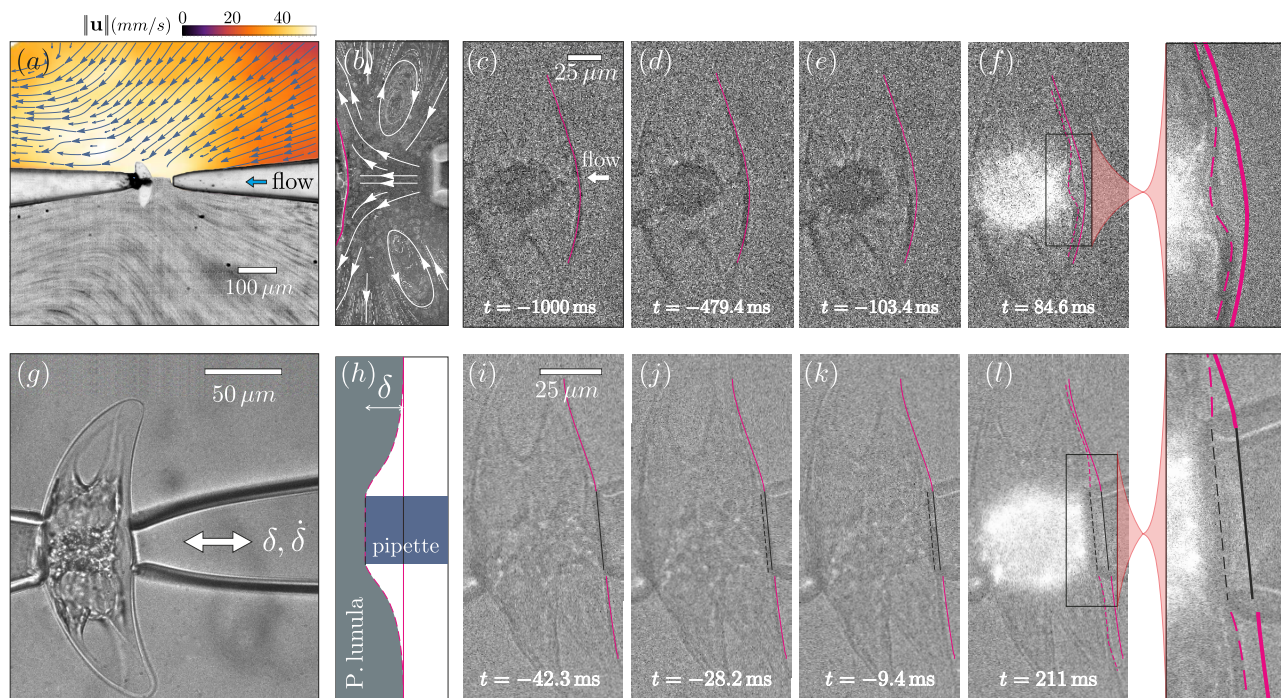


FIG. 2. Light production by *P. Lunula* under fluid and mechanical stimulation. (a) Stimulation by fluid flow; color map in upper half indicates flow speed, lower half is a streak image of tracer particles. (b) Particle tracking of flow lines near cell surface. (c-f) Cell deformation due to fluid flow and the consequent light production. (g,h) Second protocol, in which a cell is deformed under direct contact by a second pipette. (i-l) Light production triggered by mechanical deformation. All times indicated are with respect to the start of light emission.

itate micromanipulation. Its relative transparency and featureless surface allow for high-resolution imaging. As model organisms, dinoflagellates have been studied from a variety of complementary perspectives [19].

Cultures of *P. lunula* (Schütt) obtained from CCAP [20] were grown in L1 medium [21] at 20°C in an incubator on a 12h/12h light/dark cycle. The bioluminescence of *P. lunula* is under circadian regulation [22, 23] and occurs only during the night. All experiments were performed between hours 3 – 5 of the nocturnal phase. An sCMOS camera (Prime 95B, Photometrics) imaged cells through a Nikon 63 \times water-immersion objective on a Nikon TE2000 inverted microscope. Cells were kept in a $500 \mu\text{L}$ chamber that allows access by two antiparallel micropipettes held on multi-axis micromanipulators (Patchstar, Scientifica, UK) (see Supplemental Material [24]), and kept undisturbed for several hours prior to stimulation. Upon aspiration on the first pipette, cells typically flash once [25]. Care was taken to achieve consistent positioning of cells for uniformity of light measurements (Video 1 [24]).

The second pipette applies mechanical stimulation in either of two protocols. The first directs a submerged jet of growth medium at the cell, controlled by a syringe pump (PHD2000, Harvard Apparatus) and characterized using Particle Image Velocimetry (PIV) and particle tracking, as in Figs. 2a-f. Typical flow rates through

the micropipette were on the order of 1 ml/h , exiting a tip of radius $\sim 10 \mu\text{m}$, yielding maximum jet speeds U up to 1 m/s . With $\nu = \eta/\rho = 1 \text{ mm}^2/\text{s}$ the kinematic viscosity of water and $\ell \sim 0.02 \text{ mm}$ the lateral size of the organism, the Reynolds number is $Re = U\ell/\nu \sim 20$, consistent with prior studies in macroscopic flows [7, 9, 10], which utilized the apparatus scale (mm) for reference. In the second protocol, a cell is held between the two pipettes, and mechanical deformation is imposed by displacement of the second. Using the micromanipulators and a computer-controlled translation stage (DDS220/M, Thorlabs), the deformation δ and deformation rate $\dot{\delta}$ could be independently varied (Figs. 2g-l).

A key observation within the first protocol is that cells do not flash unless the imposed fluid pressure is high enough to deform the cell membrane sufficiently (Fig. 2f). For these submerged jet flows, the fluid stress $\Sigma_f \sim \rho U^2$ can be estimated to reach $\sim 10^3 \text{ Pa}$, which is the same order as in prior macroscopic experiments [7, 9, 10]. It can be seen from Fig. 2f that the lateral scale ξ of cell wall deformations is $\sim 30 \mu\text{m}$, and we estimate the fluid force exerted at the site of deformation as $F_f \sim \Sigma_f \xi^2 \sim 0.1 \mu\text{N}$. More quantitatively, using PIV of the flow field and finite-element calculations of the flow from a pipette [24] we find from study of 35 cells that the threshold for light production is broadly distributed, with a peak at $0.10 \pm 0.02 \mu\text{N}$.

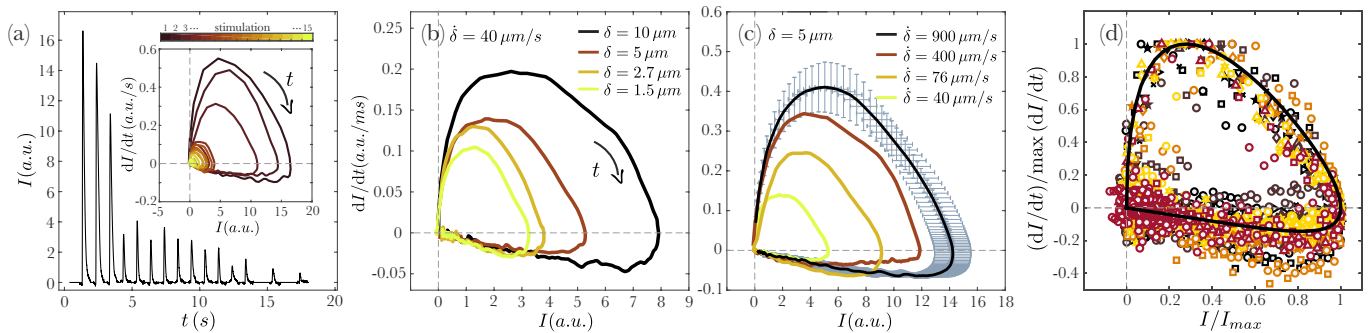


FIG. 3. Dynamics of light production following mechanical stimulation. (a) Response of a cell to repeated deformation with $\delta_f = 10 \mu\text{m}$ and $\dot{\delta} = 76 \mu\text{m/s}$. Inset: loops in $I - dI/dt$ plane for successive flashes. (b) Loops at fixed $\dot{\delta}$ and varying δ_f for first flashes. (c) As in (b), but for fixed δ_f and varying $\dot{\delta}$. Standard errors are shown for outermost data. (d) Master plot of data, normalized by maximum intensities and rates. Circles (squares) are data in b (c). Black curve is result of model in (1) and (3).

It is not clear *a priori* whether the deformations in Figs. 2c-f are resisted by the cell wall alone or also by the cytoplasm. The wall has a tough outer layer above a region of cellulose fibrils [26–28], with a thickness $d \sim 200 - 400 \text{ nm}$: AFM studies [12] show a Young’s modulus $E \sim 1 \text{ MPa}$. During asexual reproduction, the cellular contents pull away from the wall and eventually exit it through a hole, leaving behind a rigid shell with the characteristic crescent moon shape [29]. Thus, the wall is not only imprinted with that shape, but is much more rigid than the plasma membrane and significantly more rigid than the cytoplasm [12].

Deformations of such curved structures induced by localized forces involve bending and stretching of the wall. With ℓ the radius of curvature of the undeformed cell wall, a standard analysis [30] gives the indentation force $F \sim Ed^2\delta/\ell$. Balancing this against the fluid force $\rho U^2\xi^2$ we find the strain $\varepsilon \equiv \delta/\ell \sim (\rho U^2/E)(\xi/d)^2$. From the estimates above, we have $\rho U^2/E \sim 10^{-4}$, and $\xi/d \sim 50 - 100$, so ε is of the magnitude observed.

In the natural setting of marine bioluminescence and in laboratory studies of dilute suspensions, light production can arise purely from flow itself, without contact between dinoflagellates. Nevertheless, there are conceptual and methodological advantages to studying bioluminescence by direct mechanical contact, especially due to the natural compliance of cells aspirated by a single micropipette. Chief among these is the ability to control the deformation and deformation rate, which are the most natural variables for quantification of membrane stretching and bending. As seen in Fig. 2i-l, imposing deformations similar to those achieved with the fluid flow also produces bioluminescence, highlighting the role of cell membrane deformation in mechanosensing.

In our protocol for deformations, δ is increased at a constant rate $\dot{\delta}$ for a time t_f to a final value δ_f (*loading*), after which it was held fixed until any light production ceases, then returned to zero (*unloading*). We observe generally that if light is produced during loading, it is

also produced during unloading. Experiments were performed for $\delta_f \in [1, 10] \mu\text{m}$ and $\dot{\delta} \in [10, 900] \mu\text{m/s}$, with eight to twelve replicates (cells) for each data point. We repeated the given deformation protocol on the same cell (with sufficient rest intervals in between) until the cell ceases bioluminescence. Reported values of light intensity $I(t)$ are those integrated over the entire cell.

Figure 3a shows the light flashes from 15 stimulations of a single cell. With each deformation, $I(t)$ first rises rapidly and then decays on a longer time scale. Apart from a decreasing overall magnitude with successive flashes, the shape of the signal remains nearly constant. The eventual loss of bioluminescence most likely arises from exhaustion of the luciferin pool [31]. The inset shows the corresponding phase portraits of the flashes in the $I - dI/dt$ plane, where the similarity of successive signals can clearly be seen.

Focusing on the first flashes, experiments with different δ_f and $\dot{\delta}$ reveal the systematics of light production. Figures 3b&c show that for a given rate, larger deformations produce more light, as do higher rates at a given deformation. Interestingly, the shape of the signals remains the same not only between different cells but also for different mechanical stimulations; normalizing the phase portraits with respect to their maxima yields a universal shape of the signal (Fig. 3d). We summarize the results of all experiments in Figure 4a, showing the variation of maximum light intensity (averaged over all the first flashes) as a function of δ_f and $\dot{\delta}$; light production is maximized when the cell is highly deformed at high speed.

The influence of deformation and rate are suggestive of viscoelastic properties. At a phenomenological level, we thus consider a Maxwell-like model that relates the signal $s(t)$ that triggers light production to the strain ε ,

$$\dot{s} + \tau_e^{-1}s = \dot{\varepsilon}, \quad (1)$$

where τ_e is a relaxation time. For a given δ , if the deformation time scale is much smaller than τ_e , the membrane does not have time to re-arrange (the large Deborah num-

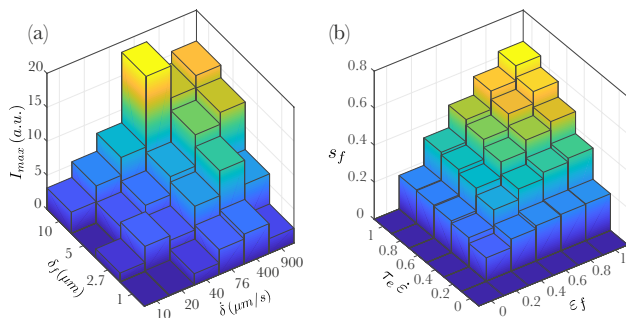


FIG. 4. Dependence of light production on deformation and rate. (a) Histogram of maximum intensity. Note nonuniform grid. (b) Variation of signal strength s_f predicted by phenomenological model, as a function of deformation and rate.

ber regime in rheology), while for slow deformations the membrane has time to relax. As seen in Figs. 2i-l and Videos 2 & 3 [24], bioluminescence occurs *during* loading, a feature that suggests τ_e is comparable to the flash rise time. Integrating (1) up to t_f , we obtain the signal s_f at the end of loading in terms of the final strain $\varepsilon_f \equiv \delta_f/\ell$ and scaled strain rate $\dot{\varepsilon}\tau_e$,

$$s_f = \dot{\varepsilon}\tau_e \left(1 - e^{-\varepsilon_f/\dot{\varepsilon}\tau_e}\right). \quad (2)$$

As seen in Fig. 4b, the peak response occurs when both the final strain and strain rate are large, as observed experimentally. The linear relationship between s and ε embodied in (1) can not continue to be valid at large strains or strain rates; eventually, the signal must saturate when all available channels open to their maximum. This is consistent with the data in Fig. 4a at the highest rates, where experimentally $\varepsilon \sim 0.25$.

Although light production is triggered internally by an action potential—which arises from nonlinear, *excitable* dynamics—analysis of the flashes [24] indicates a time course much like that of two coupled capacitors charging and discharging on different time scales. Such linear dynamics have figured in a variety of contexts, including calcium oscillations [32], bacterial chemotaxis [33], and algal phototaxis [34], and take the form of coupled equations for the observable (here, the light intensity I) which reacts to the signal s on a short time τ_r and the hidden biochemical process h which resets the system on a longer time τ_a . For light triggered by stretch-activated ion channels, the signal s might be the influx of calcium resulting from the opening of channels. Adopting units in which I, h, s are dimensionless, the simplest model is

$$\tau_r \dot{I} = s - h - I, \quad (3a)$$

$$\tau_a \dot{h} = s - h. \quad (3b)$$

Starting from the fixed point ($I = 0, h = 0$) for $s = 0$, if the signal is turned on abruptly then I will respond on a time scale τ_r , exponentially approaching $s - h \simeq s$.

Then, as h evolves toward s over the longer adaptation time scale τ_a , I will relax toward $s - h \simeq 0$, completing a flash. It follows from (3) that a discontinuous initial s creates a discontinuous \dot{I} , whereas the loops in Fig. 3 show smooth behaviour in that early regime ($I, \dot{I} \gtrsim 0$); this smoothing arises directly from the Maxwell model (1) for the signal. The parsimony of the linear model (3) comes at a cost, for it fails at very high ramp rates when $\dot{\varepsilon}$ switches to zero within the flash period and both s and I would adjust accordingly, contrary to observations. In a more complex, excitable model, the flash, once triggered, would thereafter be insensitive to the signal.

As the entire system (1) and (3) is linear, it can be solved exactly [24], thus enabling a global fit to the parameters. We compare the theoretical results with the normalized experimental data in Fig. 3d, where we see good agreement with the common loop structure. From the fits across all data, we find common time scales $\tau_e \approx 0.027$ s, $\tau_r \approx 0.012$ s, and $\tau_a \approx 0.14$ s, the last of which is comparable to the pulse decay time found in earlier experiments with mechanical stimulation [25], and can be read off directly from the late-time dynamics of the loops in Figs. 3b&c, where $\dot{I} \sim -I/\tau_a$ [24]. These values suggest comparable time scales of membrane/channel viscoelasticity and biochemical actuation, both much shorter than the decay of light flashes.

With the results described here, the generation of bioluminescence has now been explored with techniques ranging from atomic force microscope cantilevers with attached microspheres indenting cells in highly localized areas, to fluid jets and micropipette indentation on intermediate length scales, and finally to macroscopic flows that produce shear stresses across the entire cell body. Figure 5 considers all of these experiments together, organized by the perturbative stress Σ found necessary to

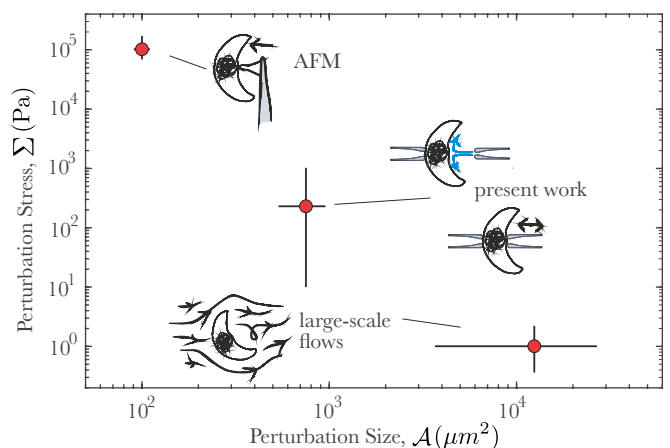


FIG. 5. Perturbation stress versus perturbation area for three kinds of experiments on dinoflagellates. Atomic force measurements on *P. lunula* are from [12], while macroscopic measurements include Taylor-Couette [7, 8] and contracting flows [9, 10] on *P. lunula* and similar dinoflagellates.

produce light and the area $\mathcal{A} \equiv \xi^2$ over which that stress was applied. We see a clear trend; the smaller the perturbation area, the larger the force required. This result suggests that the production of a given amount of light, through the triggering effects of stretch-activated ion channels on intracellular action potentials, can be achieved through the action of many channels weakly activated or a small number strongly activated. With an eye toward connecting the present results to the familiar marine context of light production, it is thus of interest to understand more quantitatively the distribution of forces over the entire cell body in strong shear flows [35] and how those forces activate ion channels to produce light. Likewise, the possible ecological significance of the great range of possible excitation scales illustrated in Fig. 5 remains to be explored.

We are grateful to Michael I. Latz for invaluable assistance at an early stage of this work, particularly with regard to culturing dinoflagellates, and thank Adrian Barbrook, Martin Chalfie, Michael Gomez, Tulle Hazelrigg, Chris Howe, Caroline Kemp, Eric Lauga, Benjamin Mauroy, Carola Seyfert, and Albane Théry for important discussions. This work was supported in part by the Gordon and Betty Moore Foundation (Grant 7523) and the Schlumberger Chair Fund. CR acknowledges support by the French government, through the UCA^{JEDI} Investments in the Future project of the National Research Agency (ANR) (ANR-15-IDEX-01).

-
- [1] E. N. Harvey, *The Nature of Animal Light*, (J.B. Lippincott Company, Philadelphia, 1920).
- [2] C. Darwin, *Journal of Researches into the Geology and Natural History of the Various Countries Visited by H.M.S. Beagle, Under the Command of Captain Fitzroy, R.N. from 1832 to 1836* (Henry Colburn, London, 1839), p. 191.
- [3] S.H.D. Haddock, M.A. Moline, and J.F. Case, Bioluminescence in the sea, *Annu. Rev. Mar. Sci.* **2**, 443 (2010).
- [4] T. Wilson, and W.J. Hastings, Bioluminescence, *Annu. Rev. Cell Dev. Biol.* **14**, 1 (1998); M. Valiadi and D. Iglesias-Rodriguez, Understanding Bioluminescence in Dinoflagellates – How Far Have We Come?, *Microorganisms* **1**, 3 (2013).
- [5] M. Fogel, and J.W. Hastings, Bioluminescence: mechanism and mode of control of scintillon activity, *Proc. Natl. Acad. Sci. USA* **69**, 3 (1972).
- [6] W. H. Biggley, E. Swift, R. J. Buchanan, and H. H. Seliger, Stimulable and spontaneous bioluminescence in the marine dinoflagellates, *Pyrodinium bahamense*, *Gonyaulax polyedra*, and *Pyrocystis lunula*, *J. Gen. Physiol.* **54**, 96 (1969); G. B. Deane, M. D. Stokes, and M. I. Latz, Bubble stimulation efficiency of dinoflagellate bioluminescence, *Luminescence* **31**, 270 (2016).
- [7] M. I. Latz, J. F. Case, and R. L. Gran, Excitation of bioluminescence by laminar fluid shear associated with simple Couette flow, *Limn. Ocean.* **39**, 1424 (1994); E.M. Maldonado and M.I. Latz, Shear-stress dependence of dinoflagellate bioluminescence, *Biol. Bull.* **212**, 242 (2007).
- [8] A.-S. Cussatlegras, and P. Le Gal, Variability in the bioluminescence response of the dinoflagellate *Pyrocystis lunula*, *J. Exp. Marine Biol. Ecol.* **343**, 74 (2007).
- [9] M. I. Latz, J. Rohr, and J. Hoyt, A novel flow visualization technique using bioluminescent marine plankton I. Laboratory studies. *IEEE J. Ocean. Eng.* **20**, 144 (1995).
- [10] M. I. Latz, A. R. Juhl, A. M. Ahmed, S. E. Elghobashi, and J. Rohr, Hydrodynamic stimulation of dinoflagellate bioluminescence: a computational and experimental study, *J. Exp. Biol.* **207**, 1941 (2004).
- [11] M. I. Latz, M. Bovard, V. VanDelinder, E. Segre, J. Rohr, and A. Groisman, Bioluminescent response of individual dinoflagellate cells to hydrodynamic stress measured with millisecond resolution in a microfluidic device, *J. Exp. Biol.* **211**, 2865 (2008).
- [12] B. Tesson, and M. I. Latz, Mechanosensitivity of a rapid bioluminescence reporter system assessed by atomic force microscopy, *Biophys. J.* **108**, 1341 (2015).
- [13] J. Rohr, J. Allen, J. Losee, and M. I. Latz, The use of bioluminescence as a flow diagnostic, *Phys. Lett. A* **228**, 408 (1997).
- [14] E. Foti, C. Faraci, R. Foti, and G. Bonanno, On the use of bioluminescence for estimating shear stresses over a rippled seabed, *Meccanica*, **45**, 881 (2010).
- [15] J. Hauslage, V. Cevik, and R. Hemmersbach, *Pyrocystis noctiluca* represents an excellent bioassay for shear forces induced in ground-based microgravity simulators (clinostat and random positioning machine), *NPJ Microgravity* **3**, 12 (2017).
- [16] G.B. Deane and M.D. Stokes, A quantitative model for flow-induced bioluminescence in dinoflagellates, *J. Theor. Bio.* **237**, 147 (2005).
- [17] K. Jin, J.C. Klima, G. Deane, M.D. Stokes, and M.I. Latz, Pharmacological investigation of the bioluminescence signaling pathway of the dinoflagellate *Lingulodinium polyedrum*: Evidence for the role of stretch-activated ion channels, *J. Phycol.* **49**, 733 (2013).
- [18] C. Kung, A possible unifying principle for mechanosensation, *Nature* **436**, 647 (2005).
- [19] J.D. Hackett, D.M. Anderson, D.L. Erdner, and D. Bhattacharya, Dinoflagellates: A remarkable evolutionary experiment, *Am. J. Bot.* **91**, 1523 (2004); C. Fajardo, *et al.*, An “omic” approach to *Pyrocystis lunula*: New insights related with this bioluminescent dinoflagellate, *J. Prot.* **209**, 103503 (2019).
- [20] The Culture Collection of Algae and Protozoa (CCAP), <https://www.ccap.ac.uk/index.htm>.
- [21] R. R. L. Guillard, and P. E. Hargraves, *Stichochrysis immobilis* is a diatom, not a chrysophyte, *Phycologia* **32**, 234 (1993).
- [22] E. Swift, and W. R. Taylor, Bioluminescence and chloroplast movement in the dinoflagellate *Pyrocystis Lunula*, *J. Phycol.* **3**, 77 (1967).
- [23] P. Colepiccolo, T. Roenneberg, D. Morse, W. R. Taylor, and J. W. Hastings, Circadian regulation of bioluminescence in the dinoflagellate *Pyrocystis Lunula*, *J. Phycol.* **29**, 173 (1993).
- [24] See Supplemental Material at <http://link.aps.org/supplemental/xxx> for further experimental details and videos.
- [25] E. A. Widder, and J. F. Case, Two flash forms in the bioluminescent dinoflagellate, *Pyrocystis fusiformis*, *J. Comp.*

- Physiol.* **143**, 43 (1981).
- [26] E. Swift and C.C. Remsen, The cell wall of *Pyrocystis* spp. (Dinococcales), *J. Phycol.* **6**, 79 (1970).
- [27] R.A. Fensome, F.J.R. Taylor, G. Norris, W.A.S. Sargeant, D.I. Wharton, and G.L. Williams, A classification of living and fossil dinoflagellates (Sheridan Press, Pennsylvania, 1993), *Micropaleontology*, Spec. Pub. No. 7.
- [28] K.S. Seo and L. Fritz, Cell-wall morphology correlated with vertical migration in the non-motile marine dinoflagellate *Pyrocystis noctiluca*, *Mar. Biol.* **137**, 589 (2000).
- [29] E. Swift and E.G. Durbin, Similarities in the asexual reproduction of the oceanic dinoflagellates, *Pyrocystis fusiformis*, *Pyrocystis lunula*, and *Pyrocystis noctiluca*, *J. Phycol.* **7**, 89 (1971).
- [30] L.D. Landau and E.M. Lifshitz, *Theory of Elasticity*, 3rd ed. (Elsevier, Amsterdam, 1986), §15.
- [31] K.S. Seo and L. Fritz, Cell ultrastructural changes correlate with circadian rhythms in *Pyrocystis lunula* (Pyrrophyta), *J. Phycol.* **36**, 2 (2000).
- [32] A. Goldbeter, G. Dupont, and M.J. Berridge, Minimal model for signal-induced Ca^{2+} oscillations and for their frequency encoding through protein phosphorylation, *Proc. Natl. Acad. Sci. USA* **87**, 1461 (1990).
- [33] P.A. Spiro, J.S. Parkinson, and H.G. Othmer, A model of excitation and adaptation in bacterial chemotaxis, *Proc. Natl. Acad. Sci. USA* **94**, 7263 (1997).
- [34] K. Drescher, R.E. Goldstein, and I. Tuval, Fidelity of adaptive phototaxis, *Proc. Natl. Acad. Sci. USA* **107**, 11171 (2010).
- [35] R. Trans-Son-Tay, S.P. Suter, G.I. Zahalak, and P.R. Rao, Membranes stresses and internal pressure in a red blood cell freely suspended in a shear flow, *Biophys. J.* **51**, 915 (1987); A. Théry, M. Jalaal, E. Lauga, and R.E. Goldstein, unpublished (2020).

SUPPLEMENTAL MATERIAL

EXPERIMENTAL SETUP

The experimental setup, shown schematically in Figure S1, consists of a microscope for visualization and positioning systems to control the two pipettes. All experiments were conducted in a darkened room. The white light illumination of the microscope (Nikon TE2000) was kept to a minimum and sent through a red long-pass filter (620 nm, Knight Optical, UK) to avoid disruption of the night phase of the dinoflagellates and to allow a greater dynamic range in capturing the bioluminescence. That background intensity was controlled in all experiments for uniformity.

Pipettes were positioned with 3D micromanipulators (Patchstar, Scientifica). For small deformation rate experiments, we used a Thorlabs 1D Direct Drive Linear Stage (DDS220/M) to control the motion. All stages were programmed with their native software. The pipettes were connected to syringes with stiff tubing and fluid flow through them could also be used to position the cells (see below). In the flow experiments, we used a syringe pump (PHD2000, Harvard Apparatus) at a constant rate. The test section was a chamber whose top and bottom were

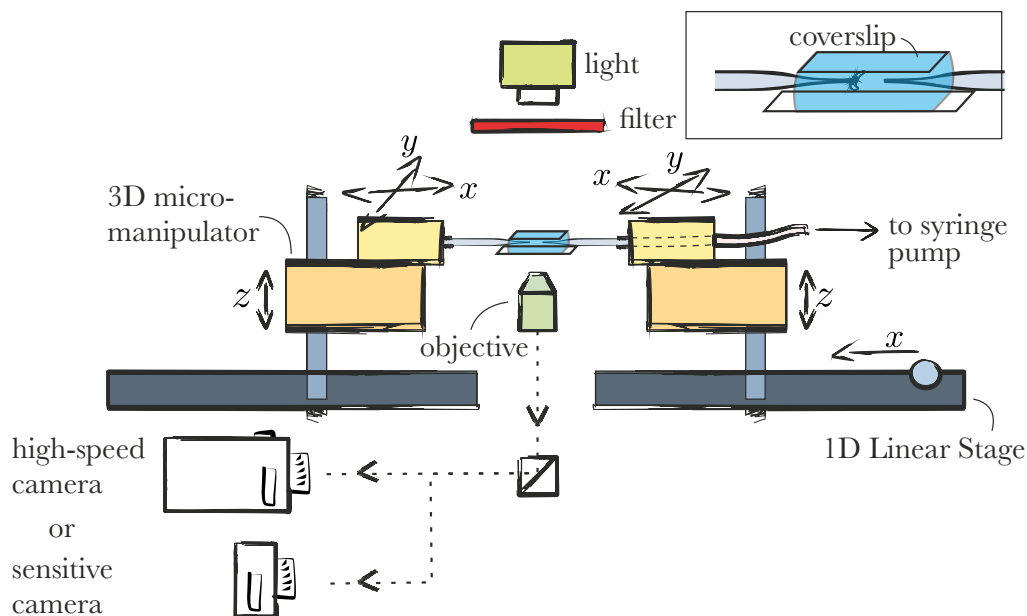


FIG. S1. Schematic of experimental setup to study bioluminescence produced by single dinoflagellates under controlled stresses.

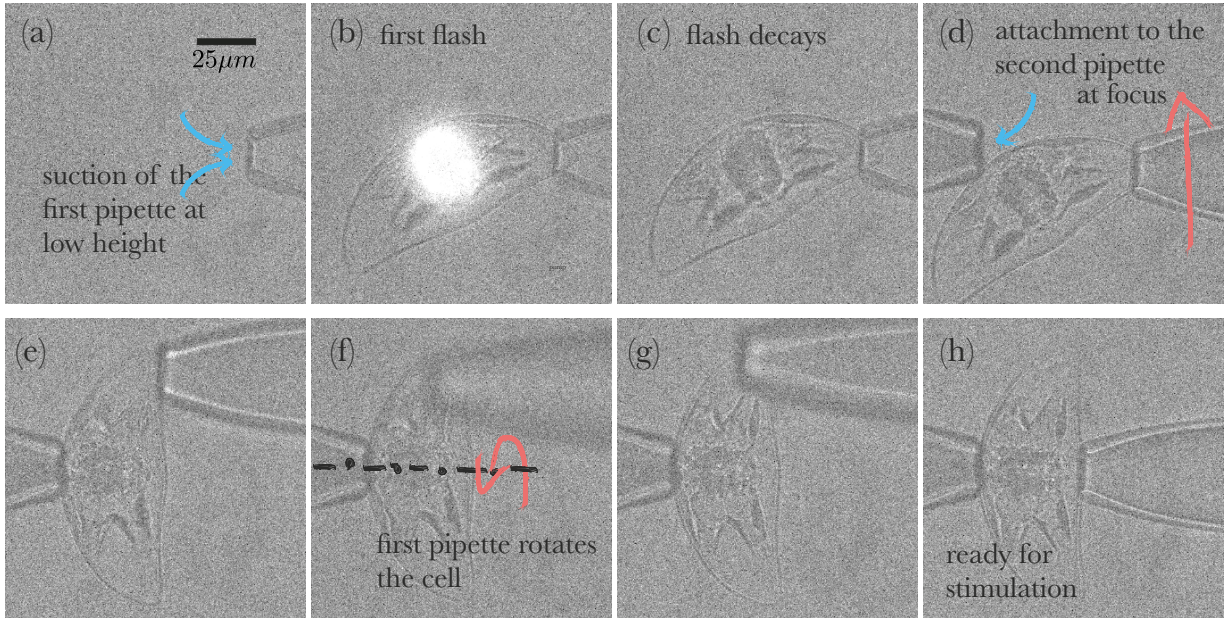


FIG. S2. Manual positioning of a cell prior to main measurements. (a) The cell is initially drawn up from the bottom cover glass using gentle flow suction. It nearly always aspirated from one of its pointy ends. The cell flashes once in this process (b) and the light decays (c). The pipettes are raised within the sample chamber to be far from the top and bottom chamber surfaces. (d) Using the joystick controllers of the micromanipulators, the cell is placed on the other pipette and then held using gentle suction (e). (f,g) The cell is rotated so that the largest area is exposed to the camera. (h) Finally, by placing the cell between the pipettes, indentation experiments can be performed.

coverslips, held apart by ~ 2 mm plastic spacers (see inset of Fig. S1). As *P. lunula* has a very characteristic three dimensional geometry, for consistency, we held the cells the same orientation within the chamber in all experiments.

As cells of *P. lunula* are negatively buoyant, they settle to the bottom coverslip of the sample chamber. Cells were positioned manually with the use of joystick controllers and gentle suction of the flow, as illustrated in Figure S2. The main bioluminescence experiments were recorded with a Prime 95B sCMOS camera (Photometrics). The high sensitivity of the camera allowed for measurements at low light condition but relatively high recording speed. For the PIV and particle tracking experiments, we used a high-speed camera (Phantom v311). Figure 1 of the main text was captured using a Nikon D810 DSLR with Differential Interference Contrast (DIC) microscopy.

SOLUTION OF THE MODEL

Equations 1, 3a and 3b are linear ODEs which can be solved exactly. As described in the main text, we take here the simplest case in which the light flash occurs within the ramp period, and therefore confine the discussion to times $t < t_f$, during which the rate of strain $\dot{\epsilon}$ is constant. From the three time constants (τ_r, τ_e, τ_a) we find τ_a to be by far the largest, and thus define the two ratios $\lambda, \rho < 1$,

$$\lambda = \frac{\tau_e}{\tau_a}, \quad \rho = \frac{\tau_r}{\tau_a}. \quad (\text{S1})$$

Then, from (1) the signal is

$$s(t) = \dot{\epsilon}\tau_e \left(1 - e^{-t/\tau_e}\right). \quad (\text{S2})$$

As $t \rightarrow 0$, $s \sim \dot{\epsilon}t + \dots$, while at long times s approaches $\dot{\epsilon}\tau_e$. If we set $t = t_f$ and note that $t_f \equiv \varepsilon_f/\dot{\epsilon}$, we obtain (2) in the main text. Substituting (S2) into (3b) and solving for h , we find

$$h = \frac{\dot{\epsilon}\tau_e}{1-\lambda} \left[1 - e^{-t/\tau_a} - \lambda \left(1 - e^{-t/\tau_e}\right)\right]. \quad (\text{S3})$$

which varies as $\dot{\epsilon}t^2/2\tau_a$ as $t \rightarrow 0$ and, as with s , approaches $\dot{\epsilon}\tau_e$ for long times.

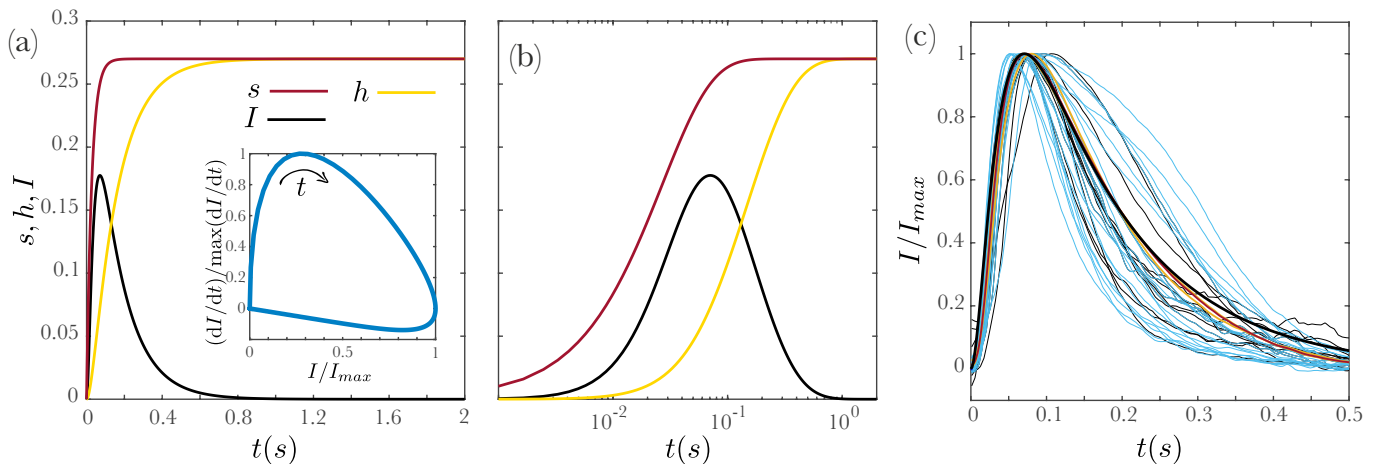


FIG. S3. a) Plots of s , h , and I for $\tau_r = 0.012$, $\tau_a = 0.14$, $\tau_e = 0.027$, and $\dot{\delta} = 500 \mu\text{m/s}$. The inset shows the phase portrait of the intensity signal. b) The same as (a) in a linear-log scale to highlight the early time behaviour. c) Intensity signals corresponding to the results shown in figure 3. Black and blue thin lines show the raw data for fixed $\dot{\delta}$ (3a) and δ (3b) and $\dot{\delta}$ (3a), respectively, and the yellow lines show their average values. The red line shows the average value of all the raw data. The black line is the same theoretical curve shown in panels a and b, normalized by its maximum value.

Finally, the light intensity is

$$I(t) = \frac{\dot{\epsilon}\tau_e}{1-\lambda} \left[\frac{1}{1-\rho} \left(e^{-t/\tau_a} - e^{-t/\tau_r} \right) - \frac{\lambda}{\lambda-\rho} \left(e^{-t/\tau_e} - e^{-t/\tau_r} \right) \right], \quad (\text{S4})$$

which behaves as $I \sim \dot{\epsilon}t^2/2\tau_r$ as $t \rightarrow 0$. At large times, with $\tau_a > \tau_e \sim \tau_r$, the dominant term in (S4) is $I \propto e^{-t/\tau_a}$, so $\dot{I} \sim -I/\tau_a$, a relationship seen in Figs. 3b&c of the main text. Figure S3 shows plots of the solutions above.

To find the time scales τ_r , τ_e and τ_a , we employed a least squares analysis on the average signal from all experiments. The values obtained, $\tau_e \approx 0.027\text{s}$, $\tau_r \approx 0.012\text{s}$, and $\tau_a \approx 0.14\text{s}$, yield the ratios $\lambda \approx 0.19$ and $\rho \approx 0.09$. Thus, the prefactors within square brackets in (S4) are $1/(1-\rho) \approx 1.1$ and $\lambda/(\lambda-\rho) \approx 1.9$. Figure S3c compares the theoretical curve for the flash intensity with the experimental data used in Figure 3 of the main text.

FINITE ELEMENT COMPUTATIONS

We performed experiments and counterpart numerical computations for 35 cells to estimate the force required for light production. The steady-state axisymmetric Navier-Stokes equations were solved numerically with the finite element software COMSOL [S1] to obtain the flow from a pipette impinging on a cell. Figure S4a shows a close up of the geometry employed. The geometry of the dinoflagellate is simplified to a sphere of radius \mathcal{R} , positioned a distance H from the outlet of the pipette. The computational domain was chosen to be sufficiently large that the presence of the domain boundaries did not affect the calculations. The inner diameter of the micropipette nozzle was set at $25 \mu\text{m}$, with a flow rate $Q = 1 \text{ ml/h}$, resulting in a fluid exit speed from the micropipette of $V \sim 1 \text{ m/s}$. Based on the actual size of the organisms, and its distance from the pipette, we performed the simulations for an average value of $\mathcal{R} = 30 \mu\text{m}$. The computations were found to be insensitive to changes in \mathcal{R} within our experimental values. The values of H varied between 9 and $75 \mu\text{m}$.

We compared PIV measurements of the flow created by the submerged jet in the absence of the dinoflagellate to the flow field computed within COMSOL, and found a good agreement. After this validation, we computed the fluid flow in the presence of the sphere (see Fig. S4) and determined the mechanical forces exerted on the surface of the dinoflagellate (sphere) by integrating the stress over its surface. By synthesizing these results with the experimental thresholds for light production we obtain in Figure S4b the probability distribution of the threshold force for bioluminescent flashes. The distribution peaks at $F_f \sim 0.1 \mu\text{N}$. This value is consistent with the estimation based on the dynamic pressure Σ_f presented in the main text.

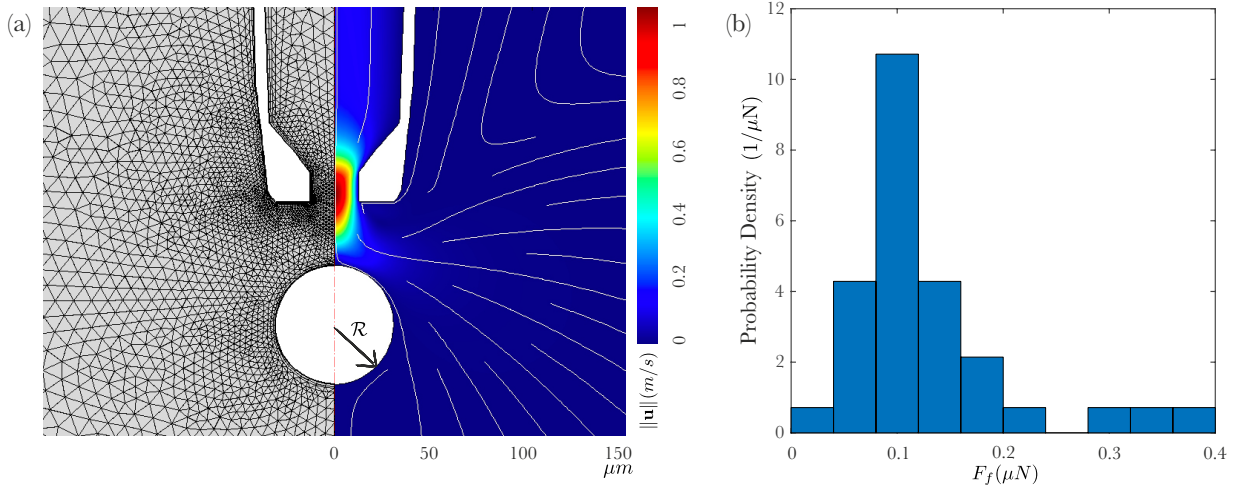


FIG. S4. (a) Numerical simulation of the fluid flow around an organism, modeled as a sphere: (left) mesh, (right) velocity magnitude. (b) Histogram of the threshold force for light production.

[S1] *COMSOL, Multiphysics v. 5.3., COMSOL AB, Stockholm, Sweden.*